

TrajFlow: Learning Distributions over Trajectories for Human Behaviour Prediction

Anna Mészáros*

Cognitive Robotics
TU Delft Netherlands

A.Meszaros@tudelft.nl

Julian F. Schumann

Cognitive Robotics
TU Delft Netherlands

J.F.Schumann@tudelft.nl

Javier Alonso-Mora

Cognitive Robotics
TU Delft Netherlands

J.AlonsoMora@tudelft.nl

Arkady Zgonnikov

Cognitive Robotics
TU Delft Netherlands
A.Zgonnikov@tudelft.nl

Jens Kober

Cognitive Robotics
TU Delft Netherlands
J.Kober@tudelft.nl

Abstract: Predicting the future behavior of human road users remains an open challenge for the development of risk-aware autonomous vehicles. An important aspect of this challenge is effectively capturing the uncertainty inherent to human behavior. This paper proposes an approach for probabilistic trajectory prediction based on normalizing flows, which provides an analytical expression of the learned distribution. We reformulate the problem of capturing distributions over trajectories into capturing distributions over abstracted trajectory features using an autoencoder, simplifying the learning task of the normalizing flows. TrajFlow improves the calibration of the learned distributions while achieving predictive performance on par with or superior to state-of-the-art methods on the ETH/UCY and the round data set.

Keywords: Normalizing Flows, Trajectory Prediction, Autonomous Vehicles

1 Introduction

Autonomous vehicles (AVs) have become an important field of research due to many promised benefits which include, but are not limited to, improved safety, accessibility, as well as reduced traffic congestion [1, 2, 3]. Yet they are still not widespread, in big part due to their inability to effectively resolve interactions with humans [4]. Being able to reliably and accurately predict human behavior in such a situation would allow for more efficient path planning while still guaranteeing safety [5].

However, predicting human behavior in traffic is complicated by the fact that such behavior is generally not deterministic, but instead stochastic, with potentially complex and multi-modal distributions [6]. An example of such a multi-modal distribution can be seen at intersections, where vehicles have the option of going left, straight, or right. While these three options are the most obvious high-level modes, there can also be other distinct modes present in data, such as sharp turns, halting in preparation for a turn, slow or fast traversals of the intersection. Such modes are scenario-dependent and may get overlooked by methods that rely on a predefined number of modes [7, 8].

Several methodologies for providing probabilistic predictions over traffic agents' future trajectories have been proposed, ranging from predicting Gaussian Mixture Models (GMMs) [7, 8] to employing generative networks. Generative networks such as Generative Adversarial Networks (GANs) [9, 10] and networks based on Variational Autoencoders (VAE) such as Conditional VAEs (CVAEs) [11, 12] and Variational Recurrent Neural Networks (VRNNs) [13, 14] are particularly interesting as they have the potential to learn complex multi-modal distributions without specifying the number of expected modes, as is necessary for methods that rely on GMMs. While those current state-of-the-art approaches already achieve good results in prediction accuracy they have the fundamental problem

of being trained to reproduce the true future trajectory, thereby ignoring the underlying stochasticity of human behavior. This training approach can result in mode collapse, which is especially problematic for GAN-based methods [9, 10]. Additionally, many state-of-the-art models predict distributions at individual time steps [11, 13], ignoring the correlation between different time steps. These kinds of predictions can lead to more conservative strategies within the subsequent motion planning [15].

To overcome these issues, one promising approach is Normalizing Flows (NFs) [16, 17], which are specifically designed to learn underlying distributions in data. While NFs can be used to learn distributions of positions at individual time steps [18, 19], more recent work has expanded to providing distributions over complete trajectories [20, 21, 22]. Even though the above NF methods already demonstrate good qualitative results in predicting multiple future trajectories, they have yet to ensure that the likelihoods inferred by the learned models are calibrated. Furthermore, for those latter models, it is also required to set the number of predicted timesteps during their design, which might limit their applicability and usefulness in an online setting.

The main contribution of this work is *TrajFlow* – an architecture for learning a prediction model with an improved calibration of the learned distribution. This is achieved through an intermediate representation of the trajectories using a Recurrent Neural Network Autoencoder, capturing the most relevant features of the trajectories and in turn also simplifying the learning of the underlying distribution. We validate our approach on a controlled data set for which we know the underlying distribution, as well as on several popular real-world data sets (ETH/UCY, rounD).

2 Background

Normalizing Flows constitute a family of generative methods which enable exact likelihood computation. They are based on the concept of transforming distributions through a series of differentiable bijective functions into a simple known “base” distribution Z_0 – most commonly a standard normal distribution.

A number of ways for constructing flow models have been proposed [23]. One possible way is by using auto-regressive flows, consisting of a series of K normalizing layers. The main components of these layers are the conditioner c_k and the transformer τ_k . In our specific case, where we chose to use a *Coupling Layer* for c_k , a *Rational Quadratic Spline* for τ_k , and a permutation layer ϵ_k , as was used in a previous model proposed by Schöller and Knoll [22] called *FloMo*. The latter two functions (τ_k and ϵ_k) are bijective – and therefore invertible – functions. In the generative direction, these functions then enable the transformation of a sample \mathbf{z}_0 from the base distribution Z_0 towards the desired distribution Z_K :

$$\mathbf{z}_{k+1} = \epsilon_k(\tau_k(\mathbf{z}_k; \boldsymbol{\theta}_k)), \quad \text{with} \quad \boldsymbol{\theta}_k = c_k(\mathbf{z}_k; \hat{\mathbf{x}}), \quad (1)$$

where \mathbf{z}_{k+1} is the result of the k -th intermediate transformation. Meanwhile, $\hat{\mathbf{x}}$ is an encoding of the observations like past trajectories, static environment, and social interactions. In the normalizing direction, F is then a composition of all K layers, where we exploit the property of c_k that $\boldsymbol{\theta}_k = c_k(\epsilon_k^{-1}(\mathbf{z}_{k+1}); \hat{\mathbf{x}})$:

$$F(\mathbf{z}_K) = (\tau_0^{-1} \circ \epsilon_0^{-1} \cdots \circ \tau_K^{-1} \circ \epsilon_K^{-1})(\mathbf{z}_K) = \mathbf{z}_0 \quad (2)$$

In the generative direction, this then allows the drawing of a sample $\mathbf{z}_K = F^{-1}(\mathbf{z}_0)$ from the desired non-normal distribution over outputs Z_K , using a sample \mathbf{z}_0 from Z_0 . The Probability Density Function (PDF) p_K of Z_K can then also be obtained in terms of the PDF p_0 :

$$\begin{aligned} p_K(\mathbf{z}_K) &= p_0(F(\mathbf{z}_K)) |\det J_F(\mathbf{z}_K)| \\ &= p_0(\mathbf{z}_0) |\det J_{F^{-1}}(\mathbf{z}_0)|^{-1}, \end{aligned} \quad (3)$$

The absolute determinant of the Jacobian $|\det J_F(\mathbf{z}_K)|$ quantifies the relative change of volume within a small neighborhood of \mathbf{z}_K when transforming it to a sample \mathbf{z}_0 using F . This ensures that the probability mass remains the same between the two distributions.

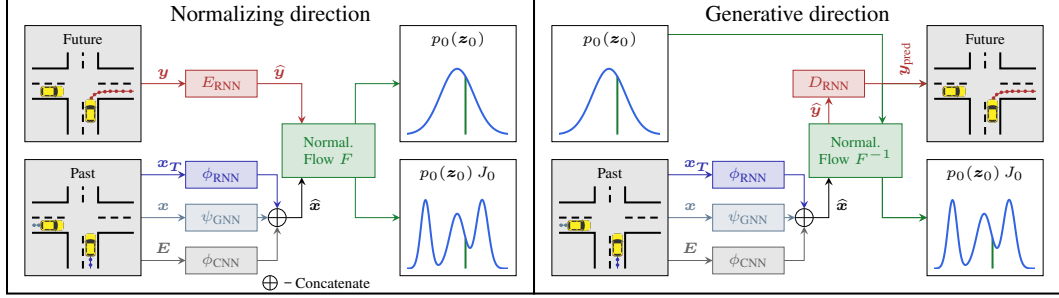


Figure 1: An overview of the TrajFlow architecture, both for the normalizing direction used during the training of the normalizing flow and the generative direction used for predicting new trajectories. The likelihood of the encoded trajectory $p_0 J_0$ uses $J_0 = |\det J_F(\hat{y})| = |\det J_{F^{-1}}(z_0)|^{-1}$. The encoding ϕ_{CNN} of map E , and the encoding ψ_{GNN} of social interactions are optional blocks, which can provide richer context information.

To learn the parameters of F , we minimize the KL-divergence between the target distribution Z_K^* with PDF $p_K^*(z_K)$ and the learned distribution Z_K with the PDF $p_K(z_K)$:

$$\begin{aligned} \mathcal{L} &= D_{\text{KL}}[p_K^*(z_K) || p_K(z_K)] \\ &= -\mathbb{E}_{z_K \sim Z_K^*} [\log p_0(F(z_K)) + \log |\det J_F(z_K)| - \log p_K^*(z_K)] \end{aligned} \quad (4)$$

With only a finite number N of samples $z_{K,n}$ representing the underlying distribution Z_K^* and ignoring the constant part $\log p_K^*(z_K)$, this loss can be approximated with:

$$\mathcal{L} \approx -\frac{1}{N} \sum_{n=1}^N \log p_0(F(z_{K,n})) + \log |\det J_F(z_{K,n})|. \quad (5)$$

3 Method: TrajFlow

We build up on the *FloMo* approach, in which NFs are employed for learning distributions directly on two-dimensional trajectories $\mathbf{y} \in \mathbb{R}^{n_O \times 2}$ defined at n_O future time steps (where $\mathbf{y} = z_K$). However, learning a distribution Z_K becomes increasingly difficult as the dimensionality of Z_K grows. Mainly, each sample z_k would become more unlikely, requiring larger data sets to fully capture the distribution over an exponentially growing domain. Additionally, as n_O in this design is fixed, the model has a limited prediction horizon, limiting its general applicability. Furthermore, people intuitively do not observe trajectories as a series of precise positions at each time step. Instead, they perceive a trajectory more abstractly in terms of general direction, length, and shape. Therefore, it can be argued that learning the distribution over such abstracted characteristics might be better suited to mimic human decision-making, an approach that has shown itself to be promising in improving prediction models [24, 25].

To overcome these challenges and to facilitate the learning of well-calibrated distributions, we construct our proposed model *TrajFlow* to let the NFs reason over such trajectory abstractions rather than the raw trajectory.

3.1 Encoding Trajectories

To capture the abstracted characteristics of a trajectory, we utilize a Recurrent Neural Network Autoencoder (RNN-AE) with encoder E_{RNN} and decoder D_{RNN} , which allows us to compress a trajectory \mathbf{y} into a lower dimensional abstraction $\hat{y} = E_{\text{RNN}}(\mathbf{y}) \in \mathbb{R}^m$ (where $m \ll 2n_O$). This addition results in the novel *TrajFlow* architecture (see Fig. 1) that consequently does not learn the distribution of future trajectories Y but rather the distribution of the encoded future trajectories \hat{Y} with $\hat{y} = z_K$.

Gated Recurrent Unit The RNN-AE uses as its main component a so-called Gated Recurrent Unit (GRU) [26], one of the main RNNs used for encoding time series events. In its most basic single-layered form with embedding dimensionality M and hidden dimensionality d , it can be depicted as a function $\phi_{\text{GRU}} : \mathbb{R}^M \times \mathbb{R}^d \rightarrow \mathbb{R}^d$, which takes at time step t an input $\mathbf{a}_t \in \mathbb{R}^M$ and uses it to change its internal hidden state $\mathbf{h} \in \mathbb{R}^d$:

$$\mathbf{h}_t = \phi_{\text{GRU}}(\mathbf{a}_t, \mathbf{h}_{t-1}) \quad (6)$$

If no hidden layer is provided at the beginning of a sequence, those can be assumed to be zero. However, *TrajFlow* employs a multi-layered version using multiple recurrent units $\phi_{\text{GRU}}^{(l)}$, with $l \in \{1, \dots, L\}$:

$$\mathbf{h}_t^{(l)} = \phi_{\text{GRU}}^{(l)}\left(\mathbf{h}_t^{(l-1)}, \mathbf{h}_{t-1}^{(l)}\right) \quad \text{with} \quad \mathbf{h}_t^{(0)} = \mathbf{a}_t \quad (7)$$

This can then be combined in a multilayer function $\phi_{\text{L-GRU}} : \mathbb{R}^M \times \mathbb{R}^{L \times d} \rightarrow \mathbb{R}^{L \times d}$ with $\mathbf{H}_t = \{\mathbf{h}_t^{(1)}, \dots, \mathbf{h}_t^{(L)}\}$:

$$\mathbf{H}_t = \phi_{\text{L-GRU}}(\mathbf{a}_t, \mathbf{H}_{t-1}) \quad (8)$$

The RNN-Encoder In the first step of the encoder E_{RNN} , we create a transformed trajectory $\tilde{\mathbf{y}} = \{\tilde{\mathbf{y}}_1, \dots, \tilde{\mathbf{y}}_{n_O}\}$ with

$$\tilde{\mathbf{y}}_t = \mathbf{y}_t - \mathbf{y}_{t-1} \quad (9)$$

This is based on previous results showing this to be more effective for trajectory prediction tasks [27]. We then use a linear layer $\phi_{\text{em}} : \mathbb{R}^2 \rightarrow \mathbb{R}^M$ that embeds a relative position $\tilde{\mathbf{y}}_t$. We then run the embedded time steps in sequence through a multi-layered GRU $\phi_{\text{E-L-GRU}}$, setting $\mathbf{a}_t = \phi_{\text{em}}(\tilde{\mathbf{y}}_t)$ in Equation (8). Using a second linear layer $\phi_{\text{E}} : \mathbb{R}^d \rightarrow \mathbb{R}^m$, we can get our final encoded trajectory $\hat{\mathbf{y}} = \phi_{\text{E}}\left(\mathbf{h}_{E,n_O}^{(L)}\right)$.

The RNN-Decoder Our decoder D_{RNN} , uses as its first step a liner layer $\phi_{\text{D}} : \mathbb{R}^m \rightarrow \mathbb{R}^M$ to pre-process an encoded trajectory $\hat{\mathbf{y}}$. We then again use a multilayer GRU $\phi_{\text{D-L-GRU}}$ (Equation (8)) to construct a new trajectory. Here, we take as our initial hidden states $\mathbf{h}_{D,0}^{(l)} = \hat{\mathbf{y}}$. Meanwhile, our input is auto-regressive, i.e. $\mathbf{a}_1 = \phi_{\text{D}}(\hat{\mathbf{y}})$ and $\mathbf{a}_t = \phi_{\text{D}}\left(\mathbf{h}_{D,t-1}^{(L)}\right)$ for $t > 1$. We construct the final relative positions using a liner layer $\phi_{\text{out}} : \mathbb{R}^d \rightarrow \mathbb{R}^2$:

$$\tilde{\mathbf{y}}_{t,\text{pred}} = \phi_{\text{out}}\left(\mathbf{h}_{D,t}^{(L)}\right) \quad (10)$$

As a last step, we then use the cumulative sum over $\tilde{\mathbf{y}}_{\text{pred}}$ to construct the predicted trajectory \mathbf{y}_{pred} (inverting Equation (9)). While we use the same hidden dimension d and embedding size M for both $\phi_{\text{E-L-GRU}}$ and $\phi_{\text{D-L-GRU}}$, we do not use any weight sharing between them.

Training The RNN-AE is trained separately before the rest of the network with a root mean square error reconstruction loss on the decoded relative positions:

$$\mathcal{L}_{\text{AE}} = \frac{1}{N} \sum_{n=1}^N \|\tilde{\mathbf{y}}_n - D_{\text{RNN}}(E_{\text{RNN}}(\tilde{\mathbf{y}}_n))\|. \quad (11)$$

During the later training of the remaining parts of the model, the weights of the RNN-AE are frozen.

3.2 Encoding Context Information

For the observations $\hat{\mathbf{x}}$, which are used for conditioning the distributions learned by the NF, we use the target agent’s past trajectory \mathbf{x}_T , the past trajectories of all agents \mathbf{x} , and optionally images of the static environment E . In order to encode these pieces of information, we use the neural networks ϕ_{RNN} , ψ_{GNN} , and ϕ_{CNN} respectively and concatenate their outputs:

$$\hat{\mathbf{x}} = \phi_{\text{RNN}}(\mathbf{x}_T) \oplus \psi_{\text{GNN}}(\mathbf{x}) \oplus \phi_{\text{CNN}}(\mathbf{E}) \quad (12)$$

An exact implementation of these components can be found in the Appendix A.

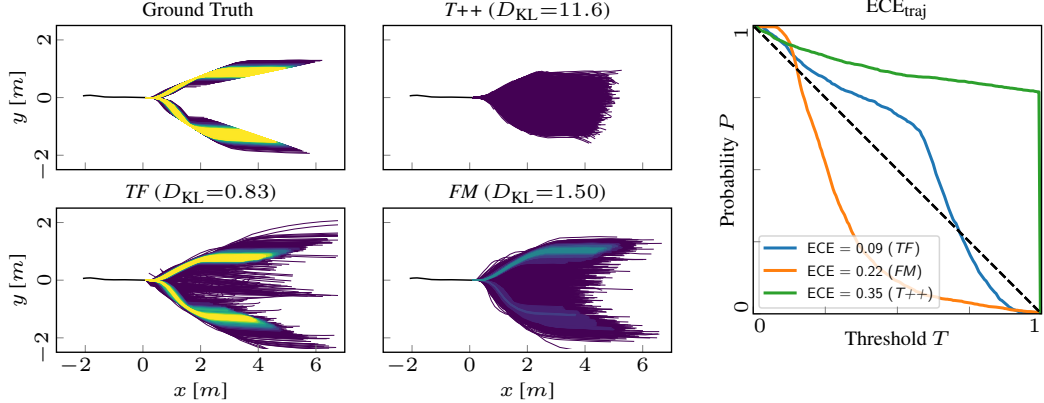


Figure 2: The left two columns depict the ground truth distribution and the distributions learned by *Trajectron++* (T++), *TrajFlow* (TF), and *FloMo* (FM) for the toy example. The colors provided in the distributions are determined based on the density values obtained through KDE on 3000 samples obtained from the respective models. The right column depicts the ECE_{traj} curves. Here, the dashed black line depicts the ideal calibration. Curves tending towards the upper right corner indicate an over-confidence or poor accuracy of the model, whereas curves tending towards the bottom left indicate an under-confidence [28].

4 Synthetic Example

We test *TrajFlow*’s ability to capture the underlying distribution of observed data on a simple bi-modal data set, in which we know the expected distribution of the future trajectories. This synthetic data set has only a single agent and no static environment information, therefore for our past observations, we use only ϕ_{RNN} .

The data set is based on two generated trajectories with distinct directions. The trajectories were split into a past sequence \mathbf{x}_i^* with $n_I = 10$ and future sequence \mathbf{y}_i^* with $n_O = 14$ recorded time steps of 0.25 s each. However, for both future trajectories, we use the same past trajectory \mathbf{x}_1^* so that the true output distribution is guaranteed to be bi-modal. With this, we avoid the learned likelihoods becoming skewed due to slight differences in the past trajectories which could in turn make it more difficult to evaluate the predicted distributions. The trajectories are then adjusted to ensure that \mathbf{x}_1^* ends at position 0. The set of future trajectories \mathbf{Y} with 3000 samples is then created by multiplying the original two futures with a random scaling factor s :

$$\mathbf{Y} = \{s_{1,i}\mathbf{y}_1^*, s_{2,i}\mathbf{y}_2^* \mid i \in 1, \dots, 1500\} \quad \text{with} \quad s \sim \mathcal{N}(1, 0.15) \quad (13)$$

We found that our approach of introducing an RNN autoencoder improves the model’s ability to capture the underlying distribution over future trajectories (Fig. 2). Compared to *FloMo* (FM), our model *TrajFlow* (TF) achieved both lower ECE_{traj} [28] and Kullback-Leibler divergence [29] (D_{KL}) values – obtained by comparing the KDE of the generated samples and the true distribution – indicating its ability to better capture the true distribution. As seen in both the predicted trajectories as well as its ECE_{traj} curve, *FloMo*’s sampled trajectories under-represent the peaks of the true distribution. Finally, it can be seen that *Trajectron++* (T++) performs significantly worse than the normalizing flow models, due to the fact that it learns distributions per time step rather than across the entire trajectory. Since the correlations between time steps are lost in this manner, the generated trajectories sometimes exhibit sudden changes in direction when transitioning from one time step to the next. This problem is especially pronounced in this data set since the variance over velocities in the y direction is exceptionally large and bi-modal.

5 Experiments

Going beyond the synthetic data set, we test our method on two real-world data sets, ETH/UCY [30, 31], and rounD [32], both of which are standard data sets used for trajectory prediction. To

facilitate those tests, we make use of a benchmarking framework developed by Schumann et al. [5], using two existing behavior prediction models as baselines: *Trajectron++* [11] and *FloMo* [22].

We use the same parameters for the NFs as the ones used in [22] for the sake of comparability between the two approaches, as *FloMo* can be considered the ablation case of *TrajFlow* for not using the RNN-AE. For the RNN-AE we use a $L = 3$ layered GRU with a hidden dimensionality $d = 4$, embedding dimensionality $M = 4$, and latent space dimensionality $m = 4$; see Section 3.1. Additionally, we employ the same ϕ_{RNN} , ψ_{GNN} , and where applicable ϕ_{CNN} for both *TrajFlow* and *FloMo*.

5.1 Data sets

Within the **ETH/UCY** pedestrian data set, 8 time steps are used for an observed trajectory in order to predict 12 time steps into the future, which amounts to 3.2 s and 4.8 s respectively, considering a sampling frequency of 2.5 Hz. Training and evaluation are performed using a leave-one-out strategy as used in [11]. Like in the majority of prior works, we do not make use of static environment information for the sake of comparability.

Within the **rounD** (Roundabout Drone) data set, 15 time steps are used for the observed past trajectory in order to predict 25 time steps into the future, which amounts to 3 s and 5 s respectively considering a sampling frequency of 5 Hz. For our evaluation, we use the scenarios extracted from the original data set as done in [33], which focus on the gap acceptance scenario of a vehicle entering the roundabout. There, both the trajectories of the vehicle entering the roundabout and the trajectory of the vehicle already inside the roundabout, which might be cut off by the former vehicle, have to be predicted. From those predicted trajectories, we extract the binary gap acceptance decision: either the vehicle outside the roundabout moves into the roundabout (accepting the gap) or waits for the other vehicle to pass (rejecting the gap). Training and evaluation are performed using a five-fold cross-evaluation strategy. For the observations, we make use of the past trajectory of the target agent, social interaction information, and an image of the scene.

5.2 Metrics

To evaluate the distance of the predicted trajectories w.r.t. the ground truth we use:

minADE/minFDE - Average/Final L_2 distance between the best-predicted trajectory and the ground truth, based on 20 predicted samples.

ADE_{ML}/FDE_{ML} - Average/Final L_2 distance between the most likely predicted trajectory and the ground truth. This trajectory is selected out of 100 predicted samples according to a PDF built using a kernel density estimate (KDE) upon those samples.

In order to obtain insight into the learned distribution over trajectories, we make use of:

Oracle 10% - Average L_2 distance per time step of the top 10 % out of 50 predicted samples with the lowest ADE [34].

KDE_{NLL} - Average Negative Log Likelihood of the ground truth, based on a KDE of the predicted distribution approximated by 100 samples.

ECE_{traj} - Expected Calibration Error for predicted trajectories, using a formulation introduced by Ivanovic et al. [28].

Lastly, in the case of classifiable behaviors, such as the gap acceptance in rounD, we use:

ECE - Expected Calibration Error for classifiers, using the specific formulation by Naeini et al. [35].

AUC - The Area Under the receiver-operator-Curve, which is robust against class biases [36].

5.3 Results

The results of our evaluations can be seen in Fig. 3 and Fig. 4, and are also summarized in tabular form in Appendix B.1. On the ETH data set, *TrajFlow* achieves comparable results to *FloMo*. The low ECE_{traj} values indicate that the NF-based models are able to capture the underlying distribution well. Meanwhile, *Trajectron++* performs overall worse across metrics, even compared to the origi-

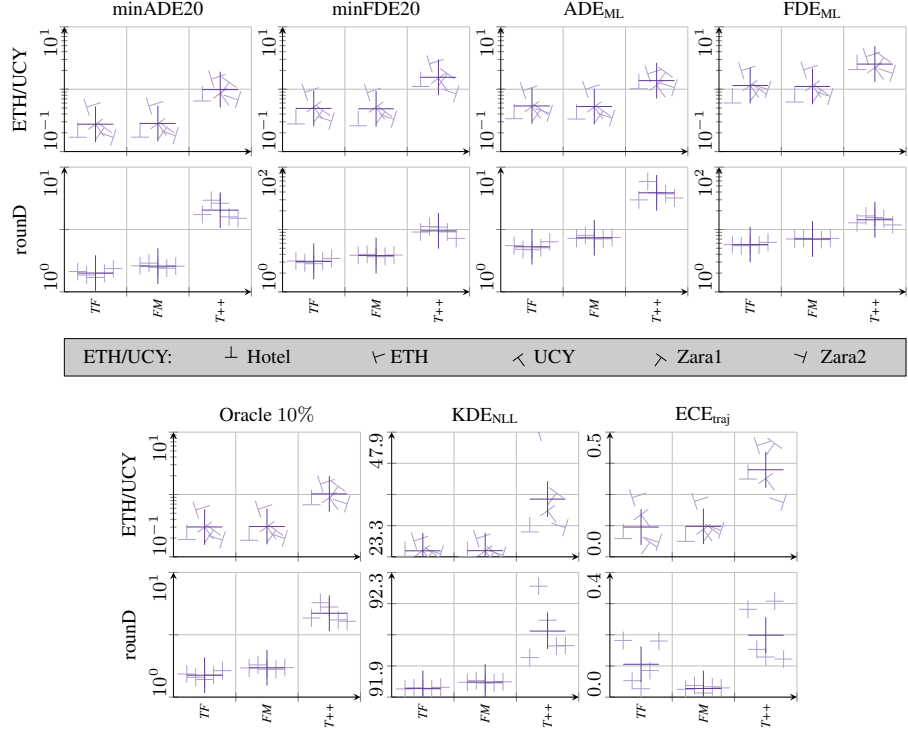


Figure 3: Results on ETH/UCY and roundD. Large crosses mark the average value of the results across all data set splits while smaller crosses and t-shaped markings – for the different test locations in the ETH/UCY data set – show the results for each of the 5 train/test splits.

nally reported values [11]. It is, however, important to note that this is not the first time the original results could not be replicated [37], and compared to common practice, we used a stricter method for extracting testing samples, necessitating the existence of all 12 future positions.

Meanwhile, on roundD, *TrajFlow* yields noticeable improvement on all distance metrics (Fig. 3), with lower ADE_{ML} / FDE_{ML} values for *TrajFlow* indicating that the predictions *TrajFlow* is most confident in lie close to the ground truth future trajectories. On the metrics which provide insight into the learned distribution itself, *TrajFlow* outperforms the other models on Oracle 10% and KDE_{NLL} . However, we observe worse performance on the ECE_{traj} metric, with our model tending to provide overconfident predictions (see Appendix B.2). While this might indicate *TrajFlow*’s poorer ability to learn the underlying distribution compared to *FloMo*, it must be noted that this metric is untested on joint prediction problems with long prediction horizons, like the one we are facing here. Consequently, the meaningfulness of the ECE_{traj} metric for this data set might be questionable, especially as *TrajFlow* surpasses the other models on the binary ECE metric with a value of 0.019 compared to 0.037 for *FloMo* and 0.067 for *Trajectron++* (see Fig. 4). Lastly, the AUC values demonstrate that *TrajFlow* is more accurate in predicting the gap acceptance behavior with an AUC of 0.995 compared to 0.991 for *FloMo* and 0.971 for *Trajectron++*.

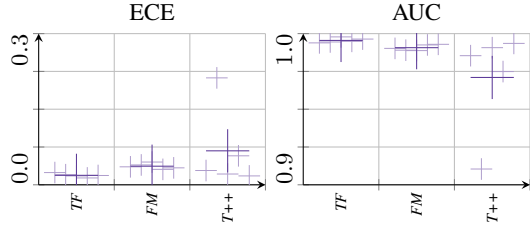


Figure 4: Gap acceptance classification results on roundD.

6 Limitations

One limitation of our approach is the auto-regressive nature of the trajectory decoder, which results in a linear increase of inference time as the number of time steps to be predicted increases. Nevertheless, this does not need to be detrimental to the use of the model in a real-world application. Real-time capability is in big part dependent on the used hardware and code optimization. Preliminary tests on a laptop PC with an NVIDIA GeForce RTX 3080 Laptop GPU and an Intel Core i9-10980HK CPU with Python code that has not been thoroughly optimized for computational efficiency enabled us to provide 100 predictions with a length of 25 time steps for an agent within 34 ms. This is well below the minimal requirement of being able to perform computations at 10 Hz. Additionally, such auto-regressive decoders make predictions over any time horizon possible.

A further limitation of the approach is that our method requires a low-dimensional representation of the desired output. Consequently, it is currently questionable whether it can be applied for predicting more complex outputs such as the evolution of an entire scene across time since a high information loss could be expected as a result of the compression to a lower-dimensional representation.

7 Conclusion

In this work, we proposed *TrajFlow*, a novel model for predicting the trajectories of human agents in traffic by applying normalizing flows to the latent space of an autoencoder trained on the future trajectories to be predicted. Through our evaluations on the ETH/UCY and round data sets, we could verify that our model is able to learn distributions within real-world data sets. *TrajFlow* achieved results comparable to state-of-the-art methods on ETH/UCY and outperformed them on round. This showed that the introduction of an RNN-AE does not lead to a degradation of our predicted trajectories despite the loss of information inherent to data compression, and in fact, for round, learning over abstracted trajectory features proved to be beneficial.

In regards to the distributions learned by the different models, we observed that the NF-based methods were able to achieve better results, while the incorporation of the RNN-AE as done in *TrajFlow* provided an additional performance boost in most cases.

7.1 Applicability to Real Systems

The proposed method makes up an important part of an AV perception–prediction–planning pipeline and has already been tested on real-world data sets. To make it applicable to real systems, it needs to be integrated with a perception module on one end and a motion planning module on the other. This requires the model to be made compatible with the most common APIs to those two modules of the AV pipeline. Measurement errors and perception uncertainty on the part of the perception model have to be considered, but might also be leveraged by the prediction model to further inform its own predictions.

To achieve the ultimate goal of developing safe AVs it is necessary that a risk-aware motion planner can determine the likelihood of collision along the entire trajectory of an agent. To achieve this one could employ a Monte Carlo (MC) sampling approach, in which a large number of trajectories are generated from the prediction model to check for collision at every time step. This approach differs from directly learning distributions over the position at individual time steps and integrating over these distributions since sampling complete trajectories would retain the correlation between time steps. An alternative to using MC sampling would be to make use of the probability density function provided by the Normalizing Flow, to integrate within the bounds of interest for the entire trajectory. For this, further work is required in understanding the structure of the trajectory encodings.

7.2 Outlook

In this work, we propose a new approach for trajectory prediction based on Normalizing Flows. By transferring the learning problem to a lower-dimensional space we were able to obtain better-

calibrated distributions, which in turn can be beneficial for further downstream tasks such as risk-aware motion planning. With promising results achieved on two real-world data sets, one with a focus on pedestrians and the other on vehicles, we intend to expand the application of our method to larger data sets. Additionally, expanding the RNN-AE to allow for joint predictions of multiple agents is also worth investigating. Finally, an important next step is the integration of *TrajFlow* with a risk-aware motion planner and later into a full perception-prediction-planning pipeline.

References

- [1] J. S. Brar and B. Caulfield. Impact of autonomous vehicles on pedestrians' safety. In *2017 IEEE 20th International Conference on Intelligent Transportation Systems (ITSC)*, pages 714–719. IEEE, 2017.
- [2] J. Meyer, H. Becker, P. M. Bösch, and K. W. Axhausen. Autonomous vehicles: The next jump in accessibilities? *Research in transportation economics*, 62:80–91, 2017.
- [3] J. Pisarov and G. Mester. The future of autonomous vehicles. *FME Transactions*, 49(1):29–35, 2021.
- [4] M. Milford, S. Anthony, and W. Scheirer. Self-driving vehicles: Key technical challenges and progress off the road. *IEEE Potentials*, 39(1):37–45, 2019.
- [5] J. F. Schumann, J. Kober, and A. Zgonnikov. Benchmarking behavior prediction models in gap acceptance scenarios. *IEEE Transactions on Intelligent Vehicles*, 2023.
- [6] G. M. Ferro and D. Sornette. Stochastic representation decision theory: How probabilities and values are entangled dual characteristics in cognitive processes. *Plos one*, 15(12):e0243661, 2020.
- [7] B. Varadarajan, A. Hefny, A. Srivastava, K. S. Refaat, N. Nayakanti, A. Cornman, K. Chen, B. Douillard, C. P. Lam, D. Anguelov, et al. Multipath++: Efficient information fusion and trajectory aggregation for behavior prediction. *arXiv preprint arXiv:2111.14973*, 2021.
- [8] K. Messaoud, N. Deo, M. M. Trivedi, and F. Nashashibi. Trajectory prediction for autonomous driving based on multi-head attention with joint agent-map representation. In *2021 IEEE Intelligent Vehicles Symposium (IV)*, pages 165–170. IEEE, 2021.
- [9] A. Gupta, J. Johnson, L. Fei-Fei, S. Savarese, and A. Alahi. Social gan: Socially acceptable trajectories with generative adversarial networks. In *Proceedings of the IEEE conference on computer vision and pattern recognition*, pages 2255–2264, 2018.
- [10] J. Amirian, J.-B. Hayet, and J. Pettré. Social ways: Learning multi-modal distributions of pedestrian trajectories with gans. In *Proceedings of the IEEE/CVF Conference on Computer Vision and Pattern Recognition Workshops*, pages 0–0, 2019.
- [11] T. Salzmann, B. Ivanovic, P. Chakravarty, and M. Pavone. Trajectron++: Dynamically-feasible trajectory forecasting with heterogeneous data. In *European Conference on Computer Vision*, pages 683–700. Springer, 2020.
- [12] Y. Yuan, X. Weng, Y. Ou, and K. M. Kitani. AgentFormer: Agent-aware transformers for socio-temporal multi-agent forecasting. In *Proceedings of the IEEE/CVF International Conference on Computer Vision*, pages 9813–9823, 2021.
- [13] B. Brito, H. Zhu, W. Pan, and J. Alonso-Mora. Social-VRNN: one-shot multi-modal trajectory prediction for interacting pedestrians. *arXiv preprint arXiv:2010.09056*, 2020.
- [14] A. Bertugli, S. Calderara, P. Coscia, L. Ballan, and R. Cucchiara. AC-VRNN: Attentive conditional-VRNN for multi-future trajectory prediction. *Computer Vision and Image Understanding*, 210:103245, 2021.
- [15] L. Janson, E. Schmerling, and M. Pavone. Monte Carlo motion planning for robot trajectory optimization under uncertainty. In *Robotics Research*, pages 343–361. Springer, 2018.
- [16] E. G. Tabak and E. Vanden-Eijnden. Density estimation by dual ascent of the log-likelihood. *Communications in Mathematical Sciences*, 8(1):217–233, 2010.
- [17] E. G. Tabak and C. V. Turner. A family of nonparametric density estimation algorithms. *Communications on Pure and Applied Mathematics*, 66(2):145–164, 2013.

- [18] N. Rhinehart, K. M. Kitani, and P. Vernaza. R2p2: A reparameterized pushforward policy for diverse, precise generative path forecasting. In *Proceedings of the European Conference on Computer Vision (ECCV)*, pages 772–788, 2018.
- [19] N. Rhinehart, R. McAllister, K. Kitani, and S. Levine. Precog: Prediction conditioned on goals in visual multi-agent settings. In *Proceedings of the IEEE/CVF Int. Conf. on Comput. Vis.*, pages 2821–2830, 2019.
- [20] A. Bhattacharyya, C.-N. Straehle, M. Fritz, and B. Schiele. Haar wavelet based block autoregressive flows for trajectories. In *DAGM German Conference on Pattern Recognition*, pages 275–288. Springer, 2020.
- [21] J. Sun, Z. Wang, J. Li, and C. Lu. Unified and fast human trajectory prediction via conditionally parameterized normalizing flow. *IEEE Robotics and Automation Letters*, 7(2):842–849, 2021.
- [22] C. Schöller and A. Knoll. FloMo: Tractable motion prediction with normalizing flows. In *IEEE/RSJ Int. Conf. Intell. Robot. Syst.*, pages 7977–7984. IEEE, 2021.
- [23] G. Papamakarios, E. T. Nalisnick, D. J. Rezende, S. Mohamed, and B. Lakshminarayanan. Normalizing flows for probabilistic modeling and inference. *J. Mach. Learn. Res.*, 22(57):1–64, 2021.
- [24] Z. Cao, E. Biyik, G. Rosman, and D. Sadigh. Leveraging smooth attention prior for multi-agent trajectory prediction. In *2022 International Conference on Robotics and Automation (ICRA)*, pages 10723–10730. IEEE, 2022.
- [25] Q. Song, W. Wang, W. Fu, Y. Sun, D. Wang, and Z. Gao. Research on quantum cognition in autonomous driving. *Scientific reports*, 12(1):300, 2022.
- [26] K. Cho, B. van Merriënboer, C. Gulcehre, D. Bahdanau, F. Bougares, H. Schwenk, and Y. Bengio. Learning phrase representations using RNN encoder–decoder for statistical machine translation. In *Proceedings of the 2014 Conference on Empirical Methods in Natural Language Processing (EMNLP)*, pages 1724–1734, Doha, Qatar, Oct. 2014. Association for Computational Linguistics. doi:10.3115/v1/D14-1179. URL <https://aclanthology.org/D14-1179>.
- [27] J. Martinez, M. J. Black, and J. Romero. On human motion prediction using recurrent neural networks. In *Proceedings of the IEEE conference on computer vision and pattern recognition*, pages 2891–2900, 2017.
- [28] B. Ivanovic, J. Harrison, and M. Pavone. Expanding the deployment envelope of behavior prediction via adaptive meta-learning. *arXiv preprint arXiv:2209.11820*, 2022.
- [29] C. M. Bishop and N. M. Nasrabadi. *Pattern recognition and machine learning*, volume 4. Springer, 2006.
- [30] S. Pellegrini, A. Ess, K. Schindler, and L. Van Gool. You’ll never walk alone: Modeling social behavior for multi-target tracking. In *2009 IEEE 12th international conference on computer vision*, pages 261–268. IEEE, 2009.
- [31] A. Lerner, Y. Chrysanthou, and D. Lischinski. Crowds by example. In *Computer graphics forum*, volume 26, pages 655–664. Wiley Online Library, 2007.
- [32] R. Krajewski, T. Moers, J. Bock, L. Vater, and L. Eckstein. The rounD dataset: A drone dataset of road user trajectories at roundabouts in germany. In *2020 IEEE 23rd International Conference on Intelligent Transportation Systems (ITSC)*, pages 1–6, 2020. doi:10.1109/ITSC45102.2020.9294728.
- [33] J. F. Schumann, A. R. Srinivasan, J. Kober, G. Markkula, and A. Zgonnikov. Using models based on cognitive theory to predict human behavior in traffic: A case study. *arXiv preprint arXiv:2305.15187*, 2023.

- [34] N. Lee, W. Choi, P. Vernaza, C. B. Choy, P. H. Torr, and M. Chandraker. Desire: Distant future prediction in dynamic scenes with interacting agents. In *Proceedings of the IEEE conference on computer vision and pattern recognition*, pages 336–345, 2017.
- [35] M. P. Naeini, G. Cooper, and M. Hauskrecht. Obtaining well calibrated probabilities using Bayesian binning. In *Proceedings of the AAAI conference on artificial intelligence*, volume 29, 2015.
- [36] J. Huang and C. X. Ling. Using auc and accuracy in evaluating learning algorithms. *IEEE Transactions on knowledge and Data Engineering*, 17(3):299–310, 2005.
- [37] F. S. Westerhout, J. F. Schumann, and A. Zgonnikov. Smooth-Trajectron++: Augmenting the Trajectron++ behaviour prediction model with smooth attention. *arXiv preprint arXiv:2305.19678*, 2023.

A The Encoding of Past Behavior

A.1 Past Trajectories

The encoder of the past behavior ϕ_{RNN} encodes the past trajectory x_T of the single target agent whose future is to be predicted, using the function $\psi_{\text{RNN},T}$. This function was taken from the implementation of Schöller and Knoll [22] and is identical to the encoder E_{RNN} (see Appendix 3.1), except that instead of $d = M = 4$ we use $d = M = 16$.

A.2 Static Environment

For encoding a gray-scale image of the static environment E , which has been rotated to align with the target agent's heading, we use a CNN function ϕ_{CNN} . For this, $L_{\text{CNN}} = 3$ convolutional layers $\phi_{\text{CNN}}^{(l)}$ are used within this network with a kernel of size 5 and a stride of 4. The first two layers additionally have a zero-padding of size 1 around the image. With this, an initial input of size $h^{(0)} \times w^{(0)} = 156 \times 257$ and $c^{(0)} = 1$ channel is transformed first into a representation with $c^{(1)} = 8$ and $h^{(1)} \times w^{(1)} = 39 \times 64$, then into a representation with $c^{(2)} = 16$ and $h^{(2)} \times w^{(2)} = 10 \times 16$ and lastly into an output representation with $c^{(3)} = 32$ and $h^{(3)} \times w^{(3)} = 2 \times 3$. This output $\phi_{\text{CNN}}^{(3)}$ is then flattened and passed through a two-layer dense network. The first linear layer transforms the input into a hidden state of length 128, while the second linear layer produces the final encoding of the image of size $M_{\text{CNN}} = 4$.

A.3 Social Interactions

To encode interactions, we use a GNN function ψ_{GNN} that processes all past trajectories $\mathbf{x} = \{\mathbf{x}_T, \mathbf{x}_1, \dots\}$. There, in the first step, the past trajectory \mathbf{x}_i of each agent i is encoded using a GRU-based function $\psi_{\text{RNN},c}$. This network is shared between all agents of each class $c \in C = \{\text{veh.}, \text{ped.}, \dots\}$, i.e. there is for instance one network $\psi_{\text{RNN}, \text{veh.}}$ to encode the past of vehicles. An embedding layer $\psi_{\text{em}} : \mathbb{R}^m \rightarrow \mathbb{R}^{M_{\text{GNN}}}$ is then applied to each encoded past trajectory, resulting in the embedded trajectory $\tilde{\mathbf{x}}_i^{(0)} = \psi_{\text{em}}(\psi_{\text{RNN},c_i}(\mathbf{x}_i))$.

In the GNN, each of the n agents is seen as a node, with n^2 unidirectional edges being established between all nodes. Based on this, L_{GNN} layers $\psi_{\text{GNN}}^{(l)}$ are applied to this network to update the nodes states $\tilde{\mathbf{x}}^{(l)} = \{\tilde{\mathbf{x}}_T^{(l)}, \tilde{\mathbf{x}}_1^{(l)}, \dots\}$:

$$\tilde{\mathbf{x}}^{(l)} = \psi_{\text{GNN}}^{(l)}(\tilde{\mathbf{x}}^{(l-1)}) \quad (14)$$

The update starts with calculating the message $\mathbf{m}_{j,i}^{(l)}$ from agent j to agent i for every possible connection, using the message network $\psi_{\text{M}} : \mathbb{R}^{2M_{\text{GNN}}+2|C|+1} \rightarrow \mathbb{R}^{M_{\text{GNN}}}$:

$$\mathbf{m}_{j,i}^{(l)} = \psi_{\text{M}}\left(\tilde{\mathbf{x}}_j^{(l-1)} \oplus \tilde{\mathbf{x}}_i^{(l-1)} \oplus \mathcal{C}_j \oplus \mathcal{C}_i \oplus \|\mathbf{x}_i - \mathbf{x}_j\|\right), \quad (15)$$

where the last three terms are the edge features between agents i and j , with $\mathcal{C}_i \in \mathbb{R}^{|C|}$ being the one-hot encoding of class c_i . Those incoming messages are then aggregated at each node:

$$\mathbf{m}_i^{(l)} = \sum_j \mathbf{m}_{j,i}^{(l)} \quad (16)$$

Lastly, the state of each node is updated, using an updated network $\psi_{\text{U}} : \mathbb{R}^{2M_{\text{GNN}}} \rightarrow \mathbb{R}^{M_{\text{GNN}}}$

$$\tilde{\mathbf{x}}_i^{(l)} = \psi_{\text{U}}^{(l)}\left(\tilde{\mathbf{x}}_i^{(l-1)} \oplus \mathbf{m}_i^{(l)}\right) + \tilde{\mathbf{x}}_i^{(l-1)} \quad (17)$$

After being propagated through all L_{GNN} layers $\psi_{\text{GNN}}^{(l)}$, the final output of ψ_{GNN} is

$$\frac{1}{n} \sum_i \tilde{\mathbf{x}}_i^{(L_{\text{GNN}})} \quad (18)$$

For our work, we chose to set $L_{\text{GNN}} = 4$ and $M_{\text{GNN}} = 32$.

B Results

B.1 Tables

We present here in tabular form the values we depicted in graph form (Fig. 3 and 4) within the main text. For every metric, the mean and standard deviation are given over all five splits. The best model in each case is underlined.

Table 1: *ETH/UCY*

Metric	Models		
	<i>TF</i>	<i>FM</i>	<i>T++</i>
minADE20 [m]	<u>0.275</u> ± 0.127	0.282 ± 0.134	0.986 ± 0.329
minFDE20 [m]	0.492 ± 0.221	<u>0.485</u> ± 0.217	1.554 ± 0.589
ADE _{ML} [m]	0.539 ± 0.215	<u>0.528</u> ± 0.243	1.374 ± 0.366
FDE _{ML} [m]	1.146 ± 0.456	<u>1.108</u> ± 0.497	2.529 ± 0.629
Oracle 10% [m]	<u>0.301</u> ± 0.138	0.306 ± 0.143	1.021 ± 0.330
KDE _{NLL}	<u>24.489</u> ± 1.050	24.519 ± 1.260	34.687 ± 7.112
ECE _{traj}	<u>0.119</u> ± 0.072	0.122 ± 0.053	0.349 ± 0.090

Table 2: *RoundD*

Metric	Models		
	<i>TF</i>	<i>FM</i>	<i>T++</i>
minADE20 [m]	<u>1.414</u> ± 0.079	1.609 ± 0.052	4.523 ± 0.632
minFDE20 [m]	<u>3.086</u> ± 0.205	3.820 ± 0.122	9.509 ± 1.440
ADE _{ML} [m]	<u>2.299</u> ± 0.126	2.716 ± 0.064	6.226 ± 0.773
FDE _{ML} [m]	<u>5.729</u> ± 0.256	7.053 ± 0.135	14.327 ± 1.743
Oracle 10% [m]	<u>1.499</u> ± 0.084	1.719 ± 0.051	4.705 ± 0.666
KDE _{NLL}	<u>91.928</u> ± 0.002	91.948 ± 0.003	92.112 ± 0.082
ECE _{traj}	0.105 ± 0.064	<u>0.028</u> ± 0.008	0.199 ± 0.080
ECE	<u>0.019</u> ± 0.003	0.037 ± 0.005	0.067 ± 0.074
AUC	<u>0.995</u> ± 0.001	0.991 ± 0.002	0.971 ± 0.031

B.2 ECE Curves

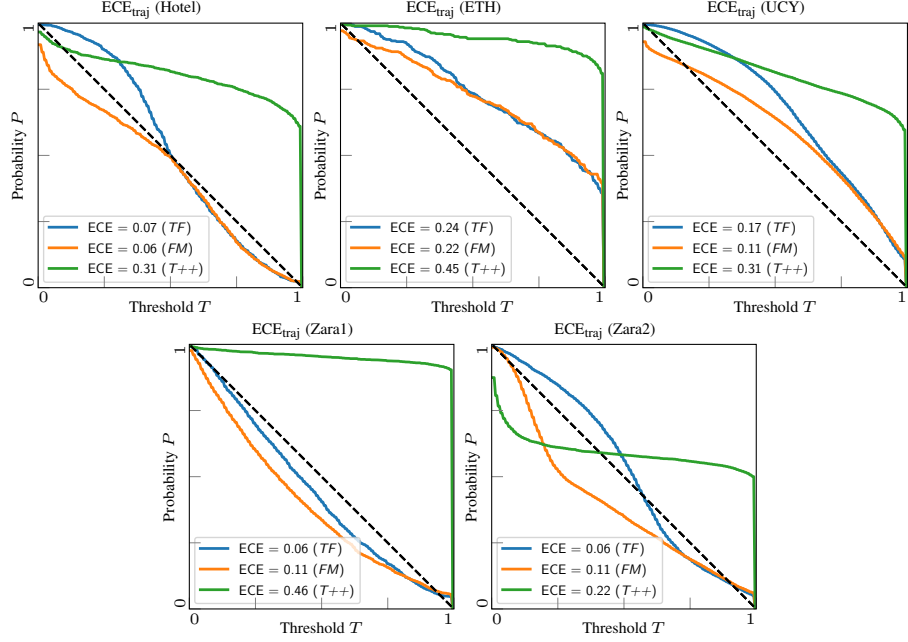


Figure 5: The ECE_{traj} metric curves on the ECE/UCY data set for all five locations.

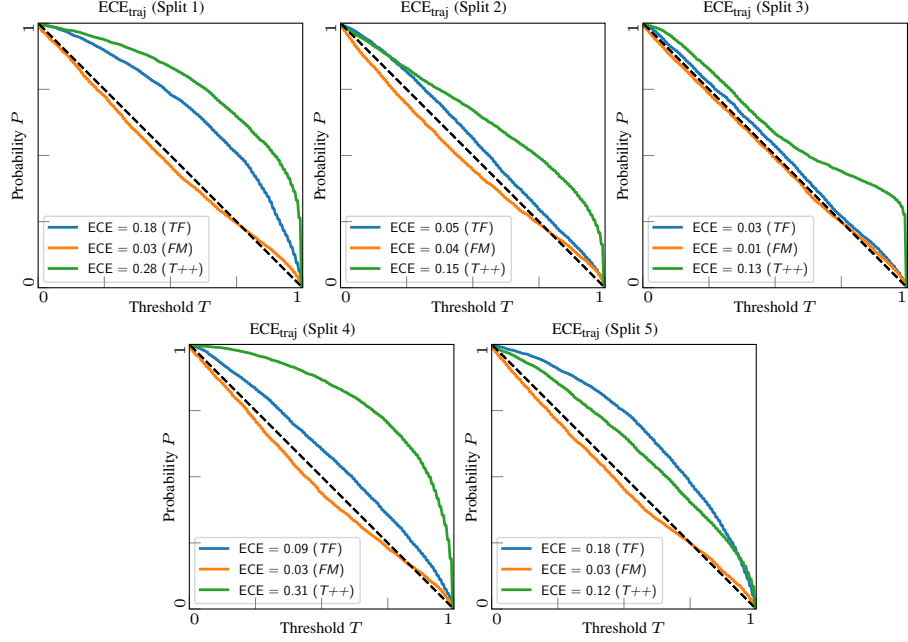


Figure 6: The ECE_{traj} metric curves on the *Round* data set for all five cross validation splits.